Photochemistry and Photobiology, 2016, 92: 231–237

Enhancing the Photocatalytic Activity of $Sr_4Al_{14}O_{25}$: Eu^{2+}, Dy^{3+} Persistent Phosphors by Codoping with Bi^{3+} Ions

Carlos R. García[1], Jorge Oliva[2], Maria Teresa Romero[1] and Luis A. Diaz-Torres*[2]

[1]Facultad de Ciencias Físico-Matemáticas,Universidad Autónoma de Coahuila, Saltillo, Mexico
[2]Grupo de Espectroscopia de Materiales Avanzados y Nanoestructurados (GEMANA), Centro de Investigaciones en Óptica, León, Mexico

Received 15 September 2015, accepted 6 December 2015, DOI: 10.1111/php.12570

ABSTRACT

The photocatalytic activity of Bismuth-codoped $Sr_4Al_{14}O_{25}$: Eu^{2+}, Dy^{3+} persistent phosphors is studied by monitoring the degradation of the blue methylene dye UV light irradiation. Powder phosphors are obtained by a combustion synthesis method and a postannealing process in reductive atmosphere. The XRD patterns show a single orthorhombic phase $Sr_4Al_{14}O_{25}$: Eu^{2+}, Dy^{3+}, Bi^{3+} phosphors even at high Bismuth dopant concentrations of 12 mol%, suggesting that Bi ions are well incorporated into the host lattice. SEM micrographs show irregular micrograins with sizes in the range of 0.5–20 μm. The samples present an intense greenish-blue fluorescence and persistent emissions at 495 nm, attributed to the 5d–4f allowed transitions of Eu^{2+}. The fluorescence decreases as Bi concentration increases; that suggest bismuth-induced traps formation that in turn quench the luminescence. The photocatalytic evaluation of the powders was studied under both 365 nm UV and solar irradiations. Sample with 12 mol % of Bi presented the best MB degradation activity; 310 min of solar irradiation allow 100% MB degradation, whereas only 62.49% MB degradation is achieved under UV irradiation. Our results suggest that codoping the persistent phosphors with Bi^{3+} can be an alternative to enhance their photocatalytic activity.

INTRODUCTION

Long persistent phosphors (LPP) are materials which can absorb energy from an excitation source, and then, when the excitation is removed, the absorbed energy is released by long persistent luminescence (1). The long persistent luminescence can last from a few minutes to several hours, this phenomenon is widely used in emergency signals, displays, decorations and recently in photocatalyst such as $TiO_{2-x}N_y$ to increase its light absorption (2–5).

The $Sr_4Al_{14}O_{25}$ host has attracted huge attention due to its strong luminescence when it is co-doped with rare earths such as Eu^{2+}, Dy^{3+} and Sm^{3+}. For example, $Sr_4Al_{14}O_{25}$: Eu^{2+}, Dy^{3+} system presents a strong greenish-blue long persistence at 490 nm (6). This emission is produced also in the $Sr_4Al_{14}O_{25}$: Eu^{2+}, but the persistence is low without the Dy^{3+} codopant, this material is considered as an efficient greenish-blue phosphor for WLEDs (7). In addition, Luitel *et al.* (8) studied the orange-red emission of the $Sr_4Al_{14}O_{25}$: Sm^{3+} phosphors and demonstrated an enhancement of that emission by co-doping with Bi, this could find possible applications in displays and lighting. However, in other systems such as Gd_2O_3: Eu^{3+}, the Bi co-dopant cause a quenching of luminescence (9). Thus, the effect of Bi codoping on luminescence properties is still unclear.

Recently, it has been reported that a blend of $Sr_4Al_{14}O_{25}$: Eu^{2+}, Dy^{3+} and the TiO_2 photocatalyst is an interesting option as photocatalyst, it can degrade toxic substances such as methylene blue due to the long persistence and strong visible absorption of the mixture of both phosphors (10). In addition, $Sr_4Al_{14}O_{25}$: Eu^{2+}, Dy^{3+} has also been mixed with Ag_3PO_4 to produce persistent photocatalysis, which allows the continuous degradation of rhodamine without the need of light (11). Nevertheless, the photocatalytic activity of the $Sr_4Al_{14}O_{25}$: Eu^{2+}, Dy^{3+} without the physical combination with other materials has not been explored to the best of our knowledge. The $Sr_4Al_{14}O_{25}$ host (without dopants) is a wide energy band gap insulator of around 5.0 eV and it absorbs mainly in the UV region (12). A general strategy to extend the absorption to the visible region of materials that absorb only UV light is by introducing dopants which can create traps into the wide band gap semiconductor (13,14). Bismuth could be an alternative for this purpose, materials with wide band gap such as TiO_2 and $BaZrO_3$ have been doped with this element, and presented a remarkable increment of absorption in the visible region; this in turn increased their photocatalytic activity (15–17). Although TiO_2 have demonstrated its effectiveness for degradation of dyes and toxic compounds, there is a controversy about the toxicity of that material for biosystems and its carcinogenic effects in humans (18,19). Furthermore, TiO_2 nanopowder has been found in some fishes such as rainbow trout and carp and this caused their death (20,21). In this sense, the search of alternative and environmental friendly photocatalysts is still a matter of research. To the best of our knowledge, there are no studies about the photocatalytic properties of $Sr_4Al_{14}O_{25}$: Eu^{2+}, Dy^{3+} doped with Bi^{3+}. Thus, the goals of this work are: (1) to demonstrate the $Sr_4Al_{14}O_{25}$: Eu^{2+}, Dy^{3+} system codoped with Bi is a good photocatalyst under ultraviolet and Sunlight irradiation and (2) to study the effect of the Bi concentration on the luminescent and photocatalytic properties of this persistent phosphor.

*Corresponding author email: ditlacio@cio.mx (Luis A. Diaz-Torres)

MATERIALS AND METHODS

Synthesis $Sr_4Al_{14}O_{25}$: Eu^{2+}, Dy^{3+} and $Sr_4Al_{14}O_{25}$: Eu^{2+}, Dy^{3+}, Bi^{3+} phosphors. Bi codoped $Sr_4Al_{14}O_{25}$: Eu^{2+}, Dy^{3+} and pure undoped $Sr_4Al_{14}O_{25}$ host samples were synthesized by a combustion synthesis method and a postannealing process in reductive atmosphere. The reagent materials: $Sr(NO_2)_3$, $Al(NO_3)_3$, $Eu(NO_3)_3$, $Dy(NO_3)_3$ and Bi $(NO_3)_3$ were acquired from Sigma Aldrich and mixed in stoichiometric proportion in water. Urea is added to the mixture to work as fuel during the combustion process. Boric acid (H_3BO_3) was added in the mixture under strong stirring in a ratio of 0.01 wt% in relation to Bi $(NO_3)_3$. Molar concentrations of Eu and Dy, were fixed at 2.0 and 1.0 mol% for all samples, except for the host sample which was pure. Samples with different Bi codopant concentrations of $x = 0.0$, 0.5, 3.0 and 12.0 mol% were produced. The combustion synthesis procedure was as follows: (1) metal nitrates were dissolved in 15 mL of deionized water under strong stirring. (2) Afterwards, urea was added and the solution was stirred for 30 min and (3) subsequently, the blend was introduced in a preheated furnace at 600°C and the combustion synthesis occurred during 30 s. As a result, a foamy material was obtained. This foam was grinded and the powders were compacted using a press to get pellets. Later, pellets were annealed at 1150°C in reducing atmosphere for 6 h. Pellets were grinded again for XRD and photocatalytic evaluation.

Structure and morphology. The crystalline structure of the obtained powders were analyzed by using a diffractometer Bruker D2, using Cu-Kα radiation ($\lambda = 1.5406$ Å). All the data obtained were between $10° < 2\theta < 60°$ in steps of 0.02° at room temperature. Scanning electron microscopy of some selected samples was analyzed by using a field-emission electron JSM-7800F microscope at room temperature using 200 kV of accelerating voltage.

Optical characterization. The absorbance spectra were obtained by using a Cary 5000 UV–VIS spectrometer in the range 200–800 nm. The photoluminescence spectra and the phosphorescent emission intensity *versus* time were taken by using an Acton Research modular spectrofluorometer. The excitation source was a 75 W Xenon lamp. The fluorescent emission from the sample was focused onto a SP-500i spectrograph (Acton Research) and detected by a photomultiplier tube R955 (Hamamatsu) connected to an Acton Research Spectra HUB and a PC collected all data. All measurements were made at room temperature.

Photocatalytic measurements. The methylene blue (MB) degradation was monitored by observing the decrease in its characteristic absorption peak at 665 nm. A solution for photocatalytic experiments was prepared in a quartz beaker by mixing 50 mL of deionized water with 1 mL of MB and 30 mg of Bi codoped $Sr_4Al_{14}O_{25}$: Eu^{2+}, Dy^{3+} powders. This solution was stirred in darkness for 1 h to allow the adsorption of the MB molecules on the surface of the photocatalyst powders. The photocatalytic experiments under UV light were carried out in a homemade photoreactor coupled with three commercial 4 W UV lamps (365 nm) in triangular configuration. The irradiance at the center of the photoreactor (where the sample is located) was 1055 ± 63 W m^{-2}. A detailed description of the photoreactor is found in reference (22). After the quartz baker with MB solution is placed in the center of the reactor, the light is turned on and solutions of 1.5 mL were regularly extracted and centrifuged. Next, the absorption spectra of the extracted solutions were taken during the photocatalytic activity experiments by using a double beam Cary-60 spectrometer in the range 200–800 nm.

The solar photocatalysis experiments were made at the astronomic observatory of Autonomous University of Coahuila in Saltillo Mexico, which coordinates are Latitude: 25°25.706′North Longitude: 100°58.616′West Height: 1581 m in a sunny day 1000–1800 h (without clouds). The solar irradiance was monitored by using a CCD Davis detector in real time and the average irradiance was 467.9 ± 36 W m^{-2}. The average of the temperature of the solution was 26.87°C and the pH of the solution at the beginning was 11 and at the end of the experiments was 10. The method to prepare the solutions for this solar photocatalysis was the same as that for the UV photocatalysis. Those solutions were exposed to the sunlight and samples of 1.5 mL were carefully extracted. Subsequently, the liquid samples were centrifuged and absorbance spectra were measured to monitor the MB absorption peak at 665 nm.

RESULTS AND DISCUSSION

Structure and morphology

$Sr_4Al_{14}O_{25}$ has an orthorhombic crystal structure with a space group of *Pmma* (51) and lattice parameters values $a = 24.785$ Å, $b = 8.487$ Å and $c = 4.866$ Å (23). Table 1 summarizes a description of samples according to their Bi molar concentrations. Figure 1 shows the XRD patterns of the undoped and $Sr_4Al_{14}O_{25}$: Eu^{2+}, Dy^{3+}, Bi^{3+} samples, with different molar concentrations of Bi^{3+}. In addition, a pure host sample $Sr_4Al_{14}O_{25}$ was produced for comparison. All diffraction peaks correspond to the $Sr_4Al_{14}O_{25}$ orthorhombic phase according to the JCPDS No. 52-1876 card. All samples show the same phase, even for high concentrations of Bi^{3+} (see sample with 12 mol%). The absence of other phases suggests that the Eu^{2+}, Dy^{3+} and Bi^{3+} dopants were successfully introduced into the $Sr_4Al_{14}O_{25}$ lattice. This also indicates that our method of preparation is robust to produce samples with high dopant concentration of Bi. It is also worthy to notice that the incorporation of Eu and Dy in the $Sr_4Al_{14}O_{25}$ host does not produce spurious phases, compare the two XRD patterns of the samples with 0% Bi in Figure 1.

SEM images of the $Sr_4Al_{14}O_{25}$: Eu^{2+}, Dy^{3+}, Bi^{3+} samples and that for the undoped sample (without Bi but with Eu and Dy) are displayed in Fig. 2a–d. The doped and the host samples are formed by irregular micrograins in the range 0.5–20 μm, and the increase in the bismuth concentration does not change the observed morphology. This range of sizes could be an advantage because the separation of our photocatalyst from water after degradation of toxic elements by simple precipitation could be possible. Some efficient photocatalysts such as TiO_2 are difficult to separate from water photocatalysis treatment due to their nanometric size (24).

Optical and luminescent properties

The absorbance spectra of the doped and host samples are shown in Fig. 3. The absorption spectra of the Bi-doped and the host samples show a peak centered at 245 nm which is related to the typical band edge absorption of the $Sr_4Al_{14}O_{25}$ host lattice (12), and is associated to an energy of around 5.0 eV. When the $Sr_4Al_{14}O_{25}$ orthorhombic lattice is co-doped with Eu^{2+} and Dy^{3+}, the absorption spectrum is extended from 300 to 460 nm. If the Bi is added, the intensity of the absorption increases, reaching a maximum in the sample with 3 mol% of Bi and then it decreases for the sample with 12 mol%. The rectangle with dashed lines drawn in Fig. 3 denotes the increase in absorption in the visible region. This increment is caused by the introduction of

Table 1. Description of samples according to the Bi-doping concentration. All samples were codoped with Eu = 1.0% and Dy = 2.0% with the exception of the pure sample.

Bi (mol%)	Powder color	Chemical formula
HOST	White	$Sr_4Al_{14}O_{25}$ (Pure)
0.0	White	$Sr_4Al_{14}O_{25}$: Eu^{2+}, Dy^{3+}
0.5	Yellow	$Sr_4Al_{14}O_{25}$: Eu^{2+}, Dy^{3+}, Bi^{3+}
3.0	Gray	$Sr_4Al_{14}O_{25}$: Eu^{2+}, Dy^{3+}, Bi^{3+}
12.0	Dark Gray	$Sr_4Al_{14}O_{25}$: Eu^{2+}, Dy^{3+}, Bi^{3+}

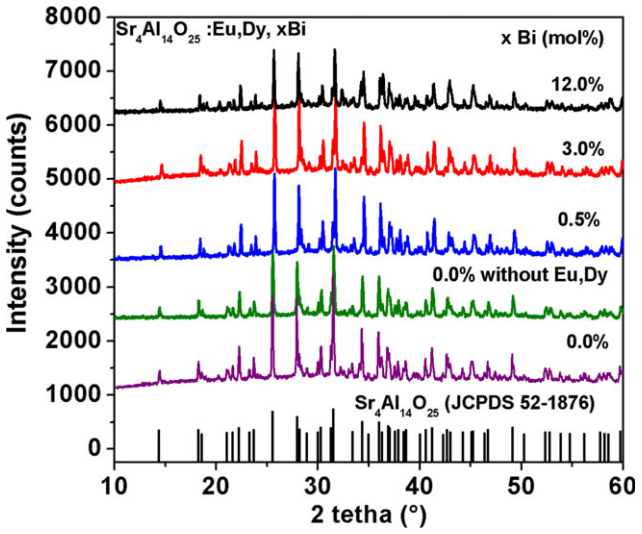

Figure 1. XRD patterns of the host sample (without dopants) and the $Sr_4Al_{14}O_{25}$: Eu^{2+}, Dy^{3+} powders doped with different Bi concentrations.

europium, dysprosium and bismuth in to the $Sr_4Al_{14}O_{25}$ host lattice. This result indicates that the presence of those ions increases the visible light absorption capabilities of the host, making it suitable for visible light photocatalysis applications. Moreover, the absorption spectra of the $Sr_4Al_{14}O_{25}$: Eu^{2+}, Dy^{3+}, Bi^{3+} phosphors show a peak absorption located at 307 nm which is attributed to the Eu–O charge transfer transition (25), and a band centered at 337 nm that corresponds to the absorption of Bi^{3+} (26). The inset in Fig. 3 depicts the Kubelka–Munk (K–M) functions *versus* energy, the energy gap (E_g) of the samples was calculated by intersecting the linear part of those curves with the axis of energy. The energy gap values for the host sample, the sample without Bi, and the 12% mol Bi-codoped sample, were 4.1, 2.9 and 2.8 eV, respectively. A decrease in the value of band gap from 4.1 to 2.9, due to the incorporation of Eu and Dy ions, corresponds to an increase in absorption range in the visible and near UV region from 250–470 nm. When Bi is incorporated, the band gap decreased a little more ranging from 2.9 to 2.8, and the absorption range of light is also increased, which makes the phosphors more suitable for the photocatalytic activity in the visible range.

Figure 4a shows the excitation and emission spectra of the $Sr_4Al_{14}O_{25}$: Eu^{2+}, Dy^{3+}, Bi^{3+}powders with different concentrations of Bi and that of the $Sr_4Al_{14}O_{25}$: Eu, Dy sample (without Bi). The sample without dopants did not present luminescence (not showed here). The excitation spectra depict a broadband ranging from 225–430 nm with a maximum excitation band centered at λ_{exc} = 370 nm and a shoulder at λ_{sh} = 310 nm. The maximum excitation at 370 nm is consistent with the transitions between the ground state $4f^7$ ($^8S_{7/2}$) and the excited state $4f^65d^1$ of the Eu^{2+} ions (27) and the shoulder at 310 nm is associated with the charge- transfer band (CTB) transition of Eu^{2+} (28,29). The emission spectra show the typical greenish-blue emission centered at 495 nm that corresponds to the allowed 5d–4f transition of Eu^{2+} ions (30–32). In addition, a weak emission at 415 nm was detected. It is well-known that the 495 nm emission corresponds to Eu^{2+} ions in the Eu(II) sites, whereas emission at 415 nm is associated to Eu^{2+} ions located in Eu(I) sites (30,31). When Eu^{2+} ions replace Sr^{2+} ions, there is no imbalance in charges because those ions have the same oxidation state +2. Moreover, the Eu (I) and Eu(II) sites are related to Sr(I) and Sr (II) inside of the orthorhombic $Sr_4Al_{14}O_{25}$ matrix (30). The Eu(I) site present the Eu^{2+} ion surrounded by AlO_4 tetrahedral

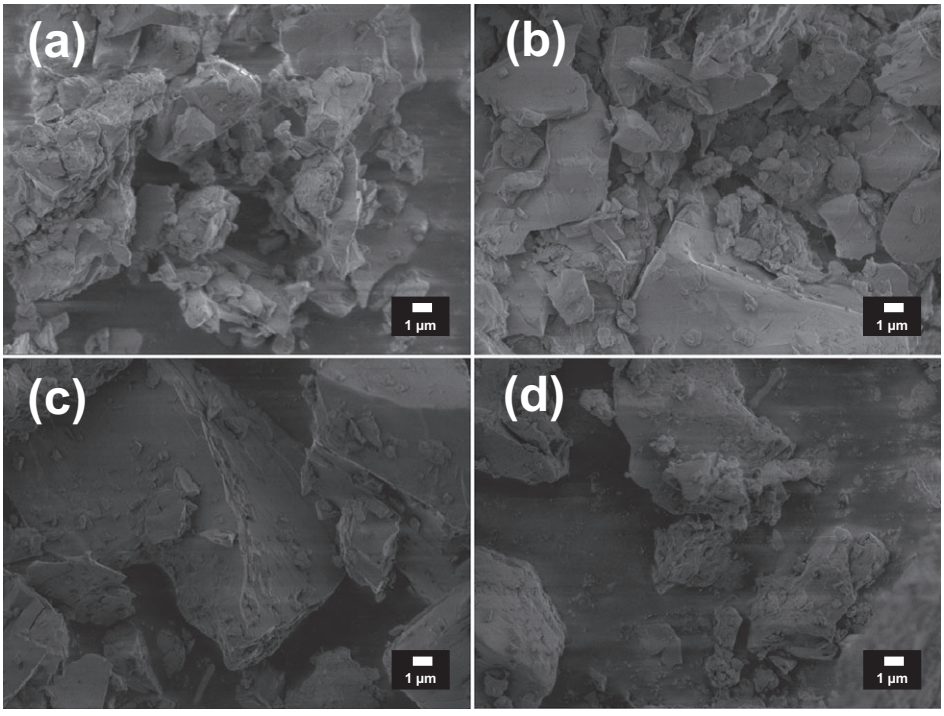

Figure 2. SEM images of: (a) $Sr_4Al_{14}O_{25}$: Eu^{2+}, Dy^{3+} powders (host without Bi) and Bi-codoped powders: (b) 0.5 mol%, (c) 3 mol% and (d) 12 mol%.

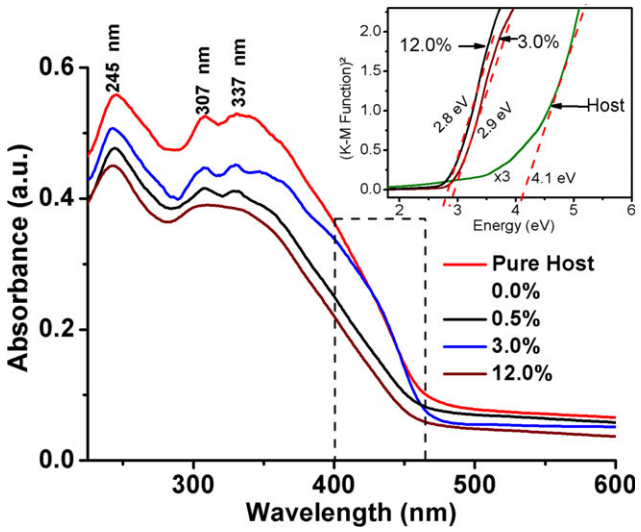

Figure 3. Absorbance spectra of the $Sr_4Al_{14}O_{25}$: Eu^{2+}, Dy^{3+} powders with different Bi concentrations and that of the pure host without dopants. The inset shows the Kubelka–Munk (K–M) functions *versus* energy for the pure host (without dopants), 0.0% Bi and 12.0% Bi-doped samples, the energy gap (E_g) of the samples was calculated by intersecting the linear part of those curves with the axis of energy.

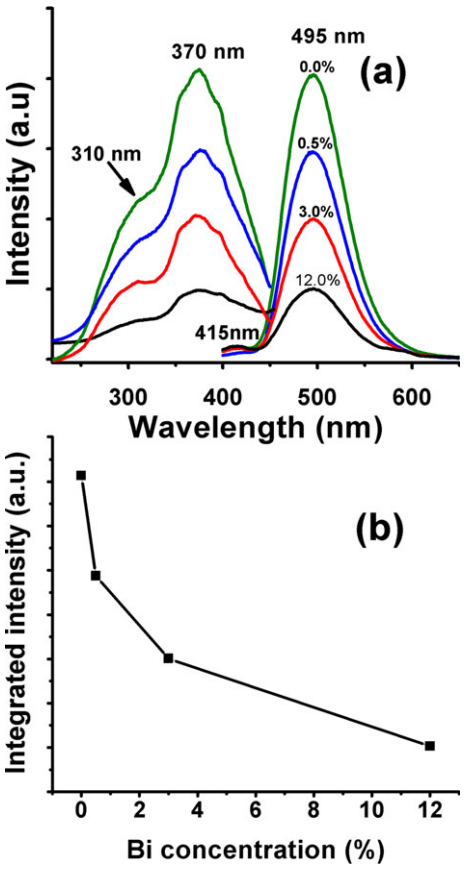

Figure 4. Excitation and emission spectra of powders with different Bismuth concentrations.

configurations and is generally associated with the 415 nm violet emission. However, for higher X concentrations of Eu^{2+} ($X \geq 1.0$ mol%), this emission disappears by the quenching effect (30). The quenching in luminescence is caused by an electrical screening when the amount of ions increase and in consequence the proximity between the ions is closer than their electronic clouds, therefore, this screening makes less probable the allowed or forbidden transitions of the rare earths (ref. [33]). When the Eu^{2+} ions are located at the Eu (II) sites, the 495 nm greenish-blue emission is present, and its crystalline environment is composed of AlO_6 octahedra which is consistent with the emission observed in our samples (refs [30,34]). Figure 4b shows a plot of integrated emission intensity as a function of Bi co-doping. It is observed that the sample doped with Eu^{2+}, Dy^{3+} and no Bi^{3+} exhibited the highest luminescence of all samples. Moreover, as the Bi concentration is increased the luminescence decreases. According to Matsukawa model (32,34), the irradiation $Sr_4Al_{14}O_{25}$: Eu^{2+}, Dy^{3+} phosphors with UV or visible light, promotes electrons from ground state $4f^7$ of the Eu^{2+} ion to the excited states $4f^65d^1$ and changes the state of Eu^{2+} ion to Eu^+. Afterwards, holes created in the ground state are thermally transferred to the ions of Dy^{3+} converting them into Dy^{4+} (32,34). When the excitation source is removed, the system relaxes and the energy is released by emitting photons of 495 nm (greenish-blue emission). Hence, if Bi^{3+} ions are present as codopants in the Dy, Eu-doped matrix ($Sr_4Al_{14}O_{25}$: Eu^{2+}, Dy^{3+}), it can create additional traps levels that correspond to a higher charge decompensation. Dy^{3+} only creates a +1 charge decompensation, when the Bi^{3+} is introduced into the $Sr_4Al_{14}O_{25}$ host the charge unbalance could be converted to +4. Therefore, this fact increase the probability to capture electrons or holes in the Bi^{3+} associated traps, which in turn reduces the probability for electrons to return to the Eu^{2+} associated traps. Consequently, these Bi traps act as quenching centers because they are near the Eu^{2+} ions in the $Sr_4Al_{14}O_{25}$ lattice located at the Eu(II) sites, therefore, a reduction in emission intensity at 495 nm is observed as Bi content increases. This is consistent with the absorbance spectrum showed in Fig. 3, since the band at 337 nm is associated with the Bi^{3+} trap levels, and this band is not observed in the samples without Bi. Figure 5 shows the phosphorescence decay time curves at 495 nm after a UV lamp (365 nm) excitation for 5 min. A dramatic decrease in phosphorescent emission intensity at the beginning (t = 0 s), as well as a decrease in the time for the persistent emission, is observed as the Bi codoping increases (compare, e.g. green and red curves in Fig. 5). The sample with the highest persistence time was the sample doped with only Eu, Dy and no Bi. This trend is consistent with previous reports (30,34). As the Bi concentration is increased, more defects (quenching centers) are introduced and those ones provoked a dramatic decrease in the intensity of the phosphorescence as is showed in Fig. 5. There is a decrease in three orders of magnitude in the emission intensity for samples with Bi concentrations ranging from 3% –12.0% after 4.5 h. In contrast, the sample without Bi had only a decrease in ~2 orders of magnitude in the emission intensity after 5 h. A photograph of selected samples is shown in Fig. 6a under natural light. The coloration of the samples is perceived at naked eye from yellow to gray as the concentration of Bi is increased, and the host (undoped) sample showed white coloration. The pellet of the $Sr_4Al_{14}O_{25}$: Eu^{2+}, Dy^{3+} sample without Bi had an intense yellow coloration and the highest phosphorescent emission. This change in coloration from yellow to gray could explain the diminution of luminescence, it has been reported that doping with bismuth from 1.0 at% and

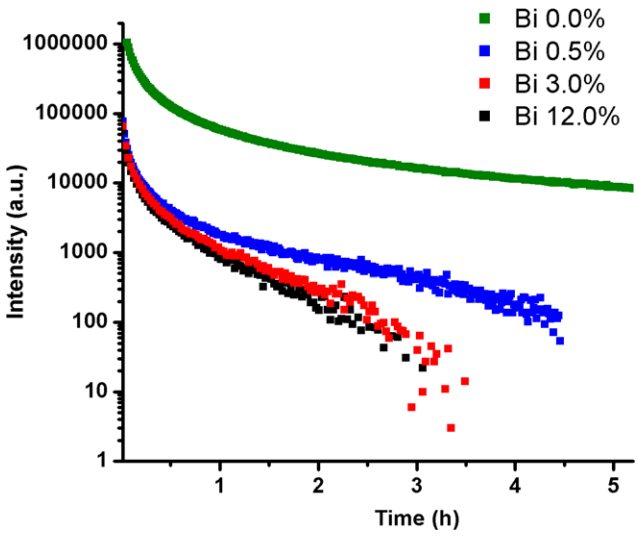

Figure 5. Curves of Phosphorescent intensity *versus* time for Bi-codoped samples.

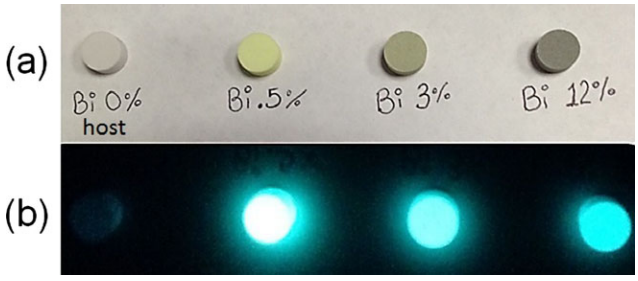

Figure 6. Pictures of the samples under (a) natural light (b) in darkness after 5 min of irradiation with the UV lamp (365 nm).

above produces a gray coloration, in our case we observed this coloration starting at the 3 mol% Bi doping. This coloration indicates the formation of bismuth centers that quench luminescence, those centers can be Bi–O polyhedra, cationic or anionic vacancies (35,36). Thus, as the concentration of Bi is increased more defects are formed and the luminescence decreases even more. After 5 min of excitation under UV light (365 nm), the light is turned off and another photograph is taken, see Fig. 6b. This one shows the phosphorescent emission in darkness. It is observed that the pure host sample do not show phosphorescence because this was not doped with Eu and Dy, however, the Bi-doped samples emit a greenish-blue luminescence and this one diminishes as the Bi concentration increases.

Photocatalytic studies

The photocatalytic activity of our samples in water was estimated using the following equation:

$$\text{Degradation } (\%) = \frac{I_t - I_0}{I_0} \times 100 \qquad (1)$$

where the I_0 and I_t are the absorbance intensity values of the MB dye solution at the beginning of the photocatalysis (samples that have not been irradiated) and the absorbance intensity after irradiation during a "t" time, respectively. Hence, a decrement in

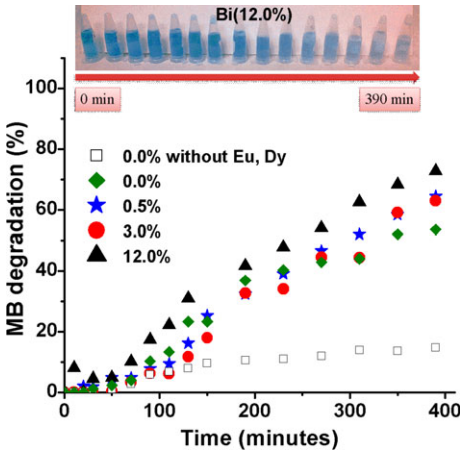

Figure 7. Degradation curve of methylene blue as a function of time under UV irradiation at 365 nm.

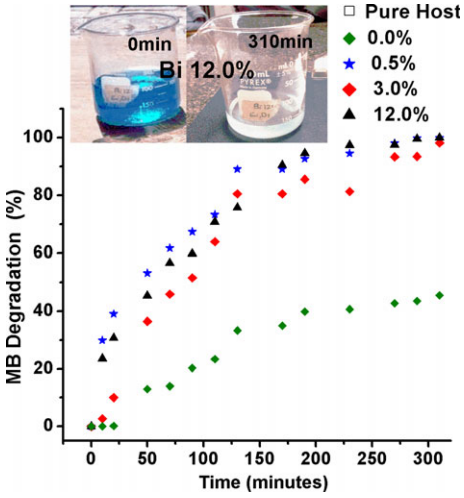

Figure 8. Degradation curve of methylene blue as a function of time under solar exposure in a sunny day in Saltillo City.

the absorbance intensity (I_t) taking as a reference the initial absorbance intensity (I_0) indicates that there is a degradation of the dye in the aqueous solutions (37).

The degradation curves of MB under UV light as a function of time are shown in Fig. 7. We observe that a continuous increment of the Bi concentration favors the photocatalytic activity. The samples doped with $x = 0.5\%$ and $x = 3.0\%$ of Bi produced ~64.0% of degradation of methylene blue after 390 min. The best sample was that one doped with $x = 12.0\%$ of Bi which produced ~75.0% of degradation after 390 min. Inset in Fig. 7 shows a picture of the sample degraded using the powders with 12% of Bi, as observed, it is still visible a light blue coloration after 390 min, indicating that the total degradation was not complete. The host sample had very low photocatalytic activity, since it degraded only 15.0% of methylene blue after 390 min. Furthermore, a comparison of the samples without Bi (see green and white curves) indicates that the presence of Eu and Dy can increase the degradation percentage ranging from 15% to 53%. This increment is caused by an enhancement of the photocatalytic activity, and this one is caused by the formation of defects (shallow traps produced by the implicit decompensation of

charge induced by the rare earth dopants) in the crystalline lattice, this in turn, reduces the recombination rate of holes and electrons and increases the lifetime of free carriers which are necessary for efficient photocatalysis (37). In general, the poor degradation of the samples without Bi is attributed to the lack of the additional defects of higher charge decompensation that Bi substitution could create. These Bi-induced traps act as better trapping centers for electrons due to their higher charge decompensation. The overall result is an increment of recombination of holes and electrons (38). When the bismuth is introduced as a dopant, the photocatalytic activity increases because its presence generates additional traps as explained before in the optical analysis. Such an increase in the photocatalytic activity can be correlated with the values of band gap. Inset in Fig. 3 shows the Kubelka–Munk plots for the samples with different concentration of Bi. As observed, the band gap decreases as the Bi concentration increases, this behavior has been observed in TiO_2 doped with Bi (15,16,34). This diminution of the values for band gap also shifts the absorption spectra toward longer wavelengths which is beneficial for photocatalysis in the visible range (39). Then, introducing the Bi^{3+} increases even more generation of free charge carriers (electrons or holes) by producing traps and this benefits the photocatalytic activity. Figure 8 shows the degradation of the methylene blue dye dissolved in water solution under natural solar irradiation using the $Sr_4Al_{14}O_{25}$: Eu^{2+}, Dy^{3+}, Bi^{3+} powders, the $Sr_4Al_{14}O_{25}$: Eu^{2+}, Dy^{3+} powders (0 mol % of Bi) and the pure host as photocatalysts. This figure illustrates that the total degradation of MB is possible after 310 min for the molar concentrations of Bi as low as 0.5%, since the samples with 0.5%, 3% and 12% produced total degradation after that time. However, the pure host sample (see white curve) had a poor degradation after 310 min (only 19%) and the sample with Dy, Eu and no Bi presented a degradation of 40% after the same time. Inset in Fig. 8 shows the solution of MB before and after 310 min and the solution is totally transparent after this time. Those results indicate that the presence of Bi is also useful to degrade MB under solar irradiation and this improvement of the degradation percentage respect to the ones obtained under UV irradiation was surely produced by the fact that the phosphors absorbed in an extended near UV to visible range when they are exposed under solar excitation. Thus, these results of photocatalytic activity under solar irradiation suggest that our Bi-codoped phosphors could be useful for applications of water cleaning under sunlight exposition in water treatment plants.

CONCLUSIONS

In summary, the simultaneous presence of Bi^{3+}, Eu^{2+} and Dy^{3+} ions is detrimental for the photoluminescent and phosphorescent properties, but benefits the photocatalytic activity of the phosphors. The presence of Bi^{3+} increases the intensity and range of absorption bands in the near UV and visible regions in comparison with the samples doped with only Eu^{2+} and Dy^{3+}. This in turn improves their photocatalytic activity. This broadening of the absorption spectra in the samples doped with Bi also produced a decrease in the values of band gap. Bi substitution in to the host lattice generates additional defects (even more than the ones produced by the solely presence of Dy and Eu ions), which in turn reduce the recombination rate of holes and electrons and increases the lifetime of free carriers which are necessary for efficient photocatalysis. Finally, total degradation of MB under solar irradiation after 310 min indicates that the $Sr_4Al_{14}O_{25}$: Eu^{2+}, Dy^{3+}, Bi^{3+}powders are good candidates for water cleaning treatments.

Acknowledgements—The author thanks the excellent technical work of C. Albor, R Valdivia, C. Mendez and M. Olmos from Centro de Investigaciones en Óptica A.C. C.R. Garcia also thanks to PRODEP-SEP 2005 Project for the support of this research.

REFERENCES

1. Tao, Q., J. Zhen-Guo, K. Zhe, L. Hong-Xia and Z. Er-Pan (2012) Preparation and optimization of long persistent luminescent $Sr_4Al_{14}O_{25}$:(Eu, Dy) phosphor materials. *J. Inorg. Mater.* **27**, 1341–1344.
2. Li, D., Y. Wang, K. Xu, L. Li, Z. Hu and H. Zhao (2015) Enhancement of photoluminescence, persistent luminescence and photocatalytic activity in $ZnGa_2O_4$ phosphors by lithium ion doping. *Opt. Mater. (Amst)* **42**, 313–318.
3. Wang, Y., K. Xu, D. Li, H. Zhao and Z. Hu (2014) Persistent luminescence and photocatalytic properties of Ga_2O_3:Cr_{3+}, Zn_{2+} phosphors. *Opt. Mater. (Amst)* **36**, 1798–1801.
4. Li, H., S. Yin, Y. Wang and T. Sato (2012) Effect of phase structures of $TiO_{2-x}N_y$ on the photocatalytic activity of $CaAl_2O_4$:(Eu, Nd)-coupled $TiO_{2-x}N_y$. *J. Catal.* **286**, 273–278.
5. Li, H., S. Yin, Y. Wang and T. Sato (2012) Persistent luminescence assisted photocatalytic properties of $CaA_{l2}O_4$:(Eu, Nd)/TiO_2-xN_y and $Sr_4Al_{14}O_{25}$:(Eu, Dy)/TiO_2-xN_y. *J. Mol. Catal. A Chem.* **363–364**, 129–133.
6. Yuan, Z.-X., C.-K. Chang, D.-L. Mao and W. Ying (2004) Effect of composition on the luminescent properties of $Sr_4Al_{14}O_{25}$: Eu^{2+}, Dy^{3+} phosphors. *J. Alloys Compd.* **377**, 268–271.
7. Wu, Z., J. Shi, J. Wang, M. Gong and Q. Su (2008) Synthesis and luminescent properties of $Sr_4Al_{14}O_{25}$:Eu^{2+} blue–green emitting phosphor for white light-emitting diodes (LEDs). *J. Mater. Sci. Mater. Electron.* **19**, 339–342.
8. Luitel, H. N., T. Watari, R. Chand, T. Torikai and M. Yada (2012) Photoluminescence properties of a novel orange red emitting $Sr_4Al_{14}O_{25}$:Sm^{3+} phosphor and PL enhancement by Bi^{3+} co-doping. *Opt. Mater. (Amst)* **34**, 1375–1380.
9. Wei, X. T., Y. H. Chen, X. R. Cheng, M. Yin and W. Xu (2010) Photoluminescence characteristics and energy transfer between Bi^{3+} and Eu^{3+} in Gd_2O_3: Eu^{3+}, Bi^{3+} nanophosphors. *Appl. Phys. B* **99**, 763–768.
10. García, C. R., L. A. Diaz-Torres, P. Salas, M. Guzman and C. Angeles-Chavez (2015) Photoluminescent and photocatalytic properties of bismuth doped strontium aluminates blended with titanium dioxide. *Mater. Sci. Semicond. Process.* **37**, 105–111.
11. Li, H., S. Yin, Y. Wang, T. Sekino, S. W. Lee and T. Sato (2013) Green phosphorescence-assisted degradation of rhodamine Bdyes by Ag_3PO_4. *J. Mater. Chem. A* **1**, 1123–1126.
12. Liepina, V., K. Smits, D. Millers, L. Grigorjeva and C. Monty (2012) The luminescent properties of persistent strontium aluminate phosphor prepared by solar induced solid state synthesis. *IOP Conf. Ser. Mater. Sci. Eng.* **38**, 012045.
13. Lin, W.-C. and Y.-J. Lin (2012) Effect of vanadium (IV)-doping on the visible light-induced catalytic activity of titanium dioxide catalysts for methylene blue degradation. *Environ. Eng. Sci.* **29**, 447–452.
14. Zhang, M., J. Wu, J. Hou and J. Yang (2013) Molybdenum and nitrogen co-doped titanium dioxide nanotube arrays with enhanced visible light photocatalytic activity. *Sci. Adv. Mater.* **5**, 535–541.
15. Wu, M.-C., J.-S. Chih and W.-K. Huang (2014) Bismuth doping effect on TiO_2 nanofibres for morphological change and photocatalytic performance. *Cryst. Eng. Comm.* **16**, 10692–10699.
16. Hu, Y., Y. Cao, P. Wang, D. Li, W. Chen, Y. He, X. Fu, Y. Shao and Y. Zheng (2012) A new perspective for effect of Bi on the photocatalytic activity of Bi-doped TiO_2. *Appl. Catal. B Environ.* **125**, 294–303.

17. Borja-Urby, R., L. A. Díaz-Torres, P. Salas, E. Moctezuma, M. Vega and C. Ángeles-Chávez (2011) Structural study, photoluminescence, and photocatalytic activity of semiconducting BaZrO3: Bi nanocrystals. *Mater. Sci. Eng., B* **176**, 1382–1387.
18. Current Intelligence Bulletin, Ocupational Exposure to Titanium Dioxide (2011) Department of Health and Human Services, Centers for Disease Control and Prevention National Institute for Occupational Safety and Health. Available at: http://www.cdc.gov/niosh/-docs/2011-160/pdfs/2011-160.pdf. Accessed on 2 November 2015.
19. Bayat, N., V. R. Lopes, J. Schölermann, L. D. Jensen and S. Cristobal (2015) Vascular toxicity of ultra-small TiO_2 nanoparticles and single walled carbon nanotubes in vitro and in vivo. *Biomaterials* **63**, 1–13.
20. Federici, G., B. J. Shaw and R. D. Handy (2007) Toxicity of titanium dioxide nanoparticles to rainbow trout (*Oncorhynchus mykiss*): gill injury, oxidative stress, and other physiological effects. *Aquat. Toxicol.* **84**, 415–430.
21. Zhang, X., H. Sun, Z. Zhang, N. Qian, Y. Chen and J. C. Crittenden (2007) Enhanced bioaccumulation of cadmium in carp in the presence of titanium dioxide nanoparticles. *Chemosphere* **67**, 160–166.
22. Rodríguez-Torres, M. D. P., L. A. Díaz-Torres, P. Salas, C. Rodríguez-González and M. Olmos-López (2014) UV photochemical synthesis of heparin-coated gold nanoparticles. *Gold Bull.* **47**, 21–31.
23. Liu, W., C. C. Lin, Y. Chiu, Y. Yeh, S. Jang and R. Liu (2011) Luminescence properties of green-emitting phosphors-$Sr_4Al_{14}O_{25}$:Eu^{2+} for LED applications. *J. Chem. Chem. Eng.* **5**, 638–643.
24. Zhao, L., T. Cui, Y. Li, B. Wang, J. Han, L. Han and Z. Liu (2015) Efficient visible light photocatalytic activity of p–n junction CuO/TiO_2 loaded on natural zeolite. *RSC Adv.* **5**, 64495–64502.
25. Cheng, B. M., C. K. Duan and P. A. Tanner (2009) Vacuum ultraviolet and visible spectra of Eu^{3+} in Y_2O_2S and Eu_2O_2S. *Opt. Mater. (Amst)* **31**, 902–904.
26. Kang, J.H., D.C., Lee, S.J., Yu and D.Y., Jeon (2006) Photoluminescence characteristics of Bi3+-sensitized YVO4:Eu3+phosphor. In *Proceedings of the 9th Asian Symposium on Information Display (ASID).* (Edited by S. Kumar), pp. 252–255. New Delhi India, 8 October–12 October 2006.
27. Yanmin, Q., Z. Xinbo, Y. Xiao, C. Yan and G. Hai (2009) Photoluminescent properties of Sr_2SiO_4:Eu^{3+} and Sr_2SiO_4:Eu^{2+} phosphors prepared by solid-state reaction method. *J. Rare Earths* **27**, 323–326.
28. Dianov, E. M. (2012) Bismuth-doped optical fibers: a challenging active medium for near-IR lasers and optical amplifiers. *Light Sci. Appl.* **1**, 1–7.
29. Chen, L., X. Deng, E. Zhao, X. Chen, S. Xue, W. Zhang, S. Chen, Z. Zhao and T. S. Chan (2014) The effect of electron cloud expansion on the red luminescence of $Sr_4Al_{14}O_{25}$:Mn^{4+} revealed by calculation of the Racah parameters. *J. Alloys Compd.* **613**, 312–316.
30. Luitel, H. N., T. Watari, R. Chand, T. Torikai and M. Yada (2013) Giant improvement on the afterglow of $Sr_4Al_{14}O_{25}$:Eu^{2+}, Dy^{3+} phosphor by systematic investigation on various parameters. *J. Mater.* **2013**, 1–10.
31. Brito, H. F., J. Hölsä, T. Laamanen, M. Lastusaari, M. Malkamäki and L. C. V. Rodrigues (2012) Persistent luminescence mechanisms: human imagination at work. *Opt. Mater. Exp.* **2**, 371–381.
32. Matsukawa, T., Y. Aoki, N. Takeuchi and Y. Murayama (1996) A new long phosphorescent phosphor with high brightness, $SrAl_2O_4$:$Eu^{2+}Dy^{3+}$. *J. Electrochem. Soc.* **143**, 2670–2673.
33. Blasse, G. and B.C. Grabmaier (1994) *Luminescent Materials*, pp. 115. Springer-Verlag, Berlin.
34. Van Den Eeckhout, K., P. F. Smet and D. Poelman (2010) Persistent luminescence in Eu^{2+}-doped compounds: a review. *Materials* **3**, 2536–2566.
35. Hou, J., R. Cao, Z. Wang, S. Jiao and H. Zhu (2012) Hierarchical nitrogen doped bismuth niobate architectures: controllable synthesis and excellent photocatalytic activity. *J. Hazard. Mater.* **217–218**, 177–186.
36. Ruan, J., L. Su, J. Qiu, D. Chen and J. Xu (2009) Bi-doped BaF_2 crystal for broadband near-infrared light source. *Opt. Exp.* **17**, 5163–5169.
37. García, C. R., J. Oliva and L. A. Díaz-Torres (2015) Photocatalytic activity of $LaSr_2AlO_5$: Eu ceramic powders. *Photochem. Photobiol.* **91**, 505–509.
38. Ma, J., J. Chu, L. Qiang and J. Xue (2012) Synthesis and structural characterization of novel visible photocatalyst Bi–TiO_2/SBA-15 and its photocatalytic performance. *RSC Adv.* **2**, 3753–3758.
39. Natarajan, T. S., K. Natarajan, H. C. Bajaj and R. J. Tayade (2013) Enhanced photocatalytic activity of bismuth-doped TiO_2 nanotubes under direct sunlight irradiation for degradation of Rhodamine B dye. *J. Nanoparticle Res.* **15**, 2–18.